Synthetic Metals 159 (2009) 1751–1756

Contents lists available at ScienceDirect

Synthetic Metals

journal homepage: www.elsevier.com/locate/synmet

Ultrafast real-time vibronic coupling dynamics of a breather soliton in *trans*-polyacetylene with a few-optical-cycle-pulse laser☆

Takayoshi Kobayashi[a,b,c,d], Takahiro Teramoto[a,b,*], Valerii M. Kobryanskii[e], Takashi Taneichi[a,b]

[a] *Department of Applied Physics and Chemistry and Institute for Laser Science, University of Electro-Communications, 1-5-1 Chofugaoka, Chofu, Tokyo 182-8585, Japan*
[b] *International Cooperative Research Project (ICORP), Japan Science and Technology Agency, 4-1-8 Honcho, Kawaguchi, Saitama 332-0012, Japan*
[c] *Department of Electrophysics, National Chiao Tung University, Hsinchu 30010, Taiwan*
[d] *Institute of Laser Engineering, Osaka University, 2-6 Yamada-oka, Suita, Osaka 565-0871, Japan*
[e] *Institute of Chemical Physics, Russian Academy of Science, Kosygin Street 4, Moscow 117977, Russia*

ARTICLE INFO

Article history:
Received 28 November 2008
Received in revised form 22 April 2009
Accepted 12 May 2009
Available online 11 June 2009

Keywords:
Ultrafast spectroscopy
Coherent vibration
Nuclear wave packets
Polymers

ABSTRACT

The dynamics preceding the spatial separation of a charged soliton pair after photoexcitation in *trans*-polyacetylene was successfully investigated by using ultrafast spectroscopy with a 6.2 fs pulse laser. It was directly verified that after photoexcitation, the electron–hole pair relaxes with a breather mode (i.e. multi-quanta vibronic states), as theory predicts, with an electron–hole pair lifetime of 33–50 fs. By applying spectrogram analysis to the time trace of the absorbance change, the ultrafast amplitude and frequency modulations of C—C and C═C stretching modes, induced by breathers and lasting no longer than 100 fs, can be observed simultaneously for the first time. The frequency shifts of both modes were in good agreement with a simulation based on the Su–Schrieffer–Heeger model. It was found that the intensities of transition dipoles changed due to breathers, whereas transition energies were dominantly modulated by C═C stretching modes as recent theoretical work predicted.

1. Introduction

Recently, rapid growth in research into applications of π conjugated polymers to optoelectronic devices has been well recognized, the interest being aroused because of high conductivity and light-emitting efficiency associated with these devices. Realistic design of novel plastic materials, with enhanced functionalities for such devices, requires deep insight into their electronic structure, charge and energy transport, and photoexcitation dynamics.

The simplest π conjugated polymer is *trans*-polyacetylene (*t*-PA). For modelling purposes, it is considered to be an infinitely long polyene. It is also well known that it has a doubly degenerate ground state and nonlinear photo-generated excitations called solitons, which arise because of the degeneracy and strong electron–phonon coupling [1–12]. The soliton dynamics after photoexcitation have been thoroughly investigated both experimentally [1,2,6–8,12] and theoretically [9–11], motivated by the high conductivity based on the soliton dynamics in the polymer chain.

The soliton dynamics in *t*-PA has been successfully interpreted about three decades ago by the Su–Schrieffer–Heeger (SSH) model [3] followed by several attempts to improve this model [10,11]. Recently, with the aid of progress in computational technology, quantum chemical approaches such as time dependent Hartree–Fock calculations have also been implemented [13,14]. All theoretical models have predicted that a breather soliton is created due to the excess energy of photoexcitation and modulates the frequencies of stretching modes of C—C and C═C bonds. This modulation is considered to last until a photo-generated electron–hole pair relaxes to an unbound charged soliton–antisoliton pair [2,3,9–12].

By utilizing an ultrashort pulse laser with 6.2 fs width, that is shorter than the C═C stretching vibration period and broadband multi-channel lock-in detector, detailed ultrafast dynamics revealing the very early-stage dynamics of soliton formation has been studied. In this paper, we present observations of the modulated wave packet real-time dynamics due to the electron–phonon coupling of the breather soliton in *t*-PA and analysed by ultrafast multi-channel pump–probe spectroscopy, finding that the results are in good agreement with recent theoretical predictions [9–14].

2. Experimental aspects

2.1. Sample

Trans-polyacetylene films were fabricated by polymerizing acetylene with a new rhenium catalyst in a highly viscous solution

☆ This paper is a proceeding of the 18th Iketani Conference.

* Corresponding author at: Department of Applied Physics and Chemistry and Institute for Laser Science, University of Electro-Communications, 1-5-1 Chofugaoka, Chofu, Tokyo 182-8585, Japan. Tel.: +81 42 443 5846; fax: +81 42 443 5826.
E-mail address: teramoto@ils.uec.ac.jp (T. Teramoto).

0379-6779/$ – see front matter © 2009 Elsevier B.V. All rights reserved.
doi:10.1016/j.synthmet.2009.05.021

of polyvinyl butyral (PVB) [15]. This synthetic method can provide soluble compositions containing nanoparticles of polyacetylene in PVB solution. These nanoparticles with diameters of 15–30 nm contain only a negligibly low concentration of conformational and chemical defects in contrast to those obtained by conventional methods of polyacetylene synthesis [16]. They are extremely stable even under atmospheric conditions and exhibit a number of unique optical properties such as large Raman cross-section, thermochromism, and a transparent band in the optical spectrum in the near-infrared field [16].

2.2. Ultrafast spectroscopy

Both pump and probe pulses were derived from a non-collinear optical parametric amplifier (NOPA) system developed in our group [17,18]. The pump source of this system is a regenerative amplifier (Spectra-Physics, Spitfire). The visible NOPA pulse was 6.2 fs in duration and covered a photon energy range of 1.69–2.37 eV, with constant spectral phase throughout the whole laser spectrum. Pump–probe signals were detected with a 128-channel lock-in amplifier. Real-time vibrational spectra were measured at delay times between pump (40 nJ) and probe pulses (2 nJ) from −100 fs to 1100 fs with 1-fs increments.

3. Results and discussion

3.1. Primary energy relaxation process

Fig. 1 displays the stationary absorption spectrum of *t*-PA showing a strong absorption in the visible region due to interband intrachain dipole allowed $\pi \rightarrow \pi^*$ transitions. The peak wavelength (photon energy) of 630 nm (1.97 eV) in the spectra corresponds to the ^1B_u state [19]. The laser spectrum is also shown in Fig. 1. The overlap of the spectra of laser and sample absorption is very good.

Using the femtosecond laser and multi-channel detection system described in Section 2, the time-resolved spectra of a *t*-PA sample film were measured. The results of the pump–probe experiment are shown in Fig. 2(a). Fig. 2 depicts the three-dimensional display of real-time difference absorption spectrum, $\Delta A(\omega, t)$, of over the spectral range from 528 nm (2.35 eV) to 730 nm (1.70 eV) extending from the delay time of −100 fs to 1100 fs. The modulations of $\Delta A(\omega, t)$ due to molecular vibrations can be seen clearly in Fig. 2(b) which is a expanded view of Fig. 2(a) in the time range from 0 fs to 300 fs. Fig. 2(c) show the real-time traces of $\Delta A(t)$ at the photon energies of 1.86 eV, 1.96 eV, and 2.12 eV, and Fig. 2(c) depicts the difference absorption spectrum, $\Delta A(\omega)$, at the delay times of 40 fs, 60 fs, and 120 fs.

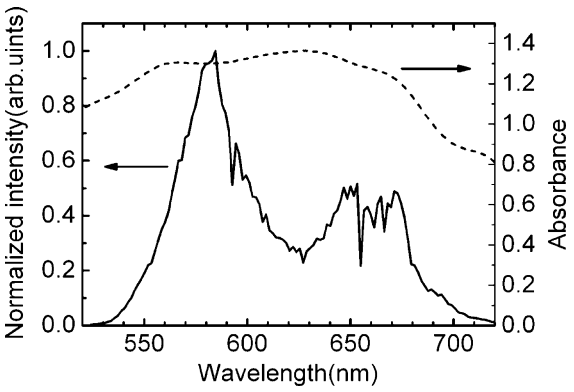

Fig. 1. Laser spectrum (solid line) and stationary absorption (dotted line) spectrum of *t*-PA.

The three-dimensional difference absorption spectra $\Delta A(\omega, t)$ were decomposed into phenomenological components of three difference spectra $\Delta A_1(\omega)$, $\Delta A_2(\omega)$, and $\Delta A_3(\omega)$ with a set of three corresponding decay time constants, τ_1, τ_2, and τ_3, by a global fitting method as given by the following equation:

$$\Delta A(\omega, t) = \Delta A_1(\omega) \exp\left(\frac{-t}{\tau_1}\right) + \Delta A_2(\omega) \exp\left(\frac{-t}{\tau_2}\right) + \Delta A_3(\omega) \exp\left(\frac{-t}{\tau_3}\right) \quad (1)$$

The decay times of the signal were determined by the singular value decomposition method to be $\tau_1 = 66 \pm 20$ fs, $\tau_2 = 565 \pm 50$ fs, and $\tau_3 \gg 2$ ps, by fitting Eq. (1) to the absorption spectra over the whole probe photon energy region. The shortest time constant, τ_1, is the lifetime of the electron–hole pair, which is in good agreement with values found in the literature [8,13,14]. The medium length decay time τ_2 corresponds to the lifetime of a charged soliton–antisoliton pair to geminate recombination [8]. The absolute value of the longest time constant τ_3 cannot be determined,

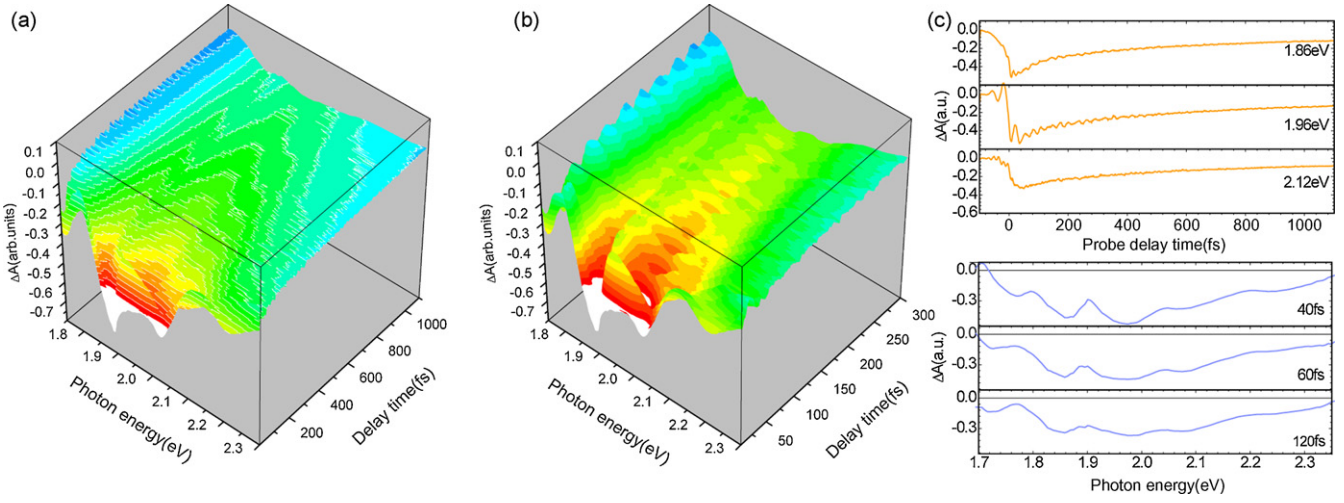

Fig. 2. Three-dimensional real-time absorbance change spectrum of *t*-PA: (a) three-dimensional display of $\Delta A(\omega, t)$ of *t*-PA over the spectral range from 528 nm (2.35 eV) to 730 nm (1.70 eV) extending from delay time of −100 fs to 1100 fs; (b) expanded view of (a) in the time range of 0–300 fs. (c) The upper three show the real-time traces of ΔA at photon energy 1.86 eV, 1.96 eV, and 2.12 eV, respectively. The lower three show the photon energy dependencies of ΔA at delay time 40 fs, 60 fs, and 120 fs, respectively.

only a lower limit being obtained. However, this time constant is considered to be associated with the thermalization of the system, which does not necessarily have to be described with a single exponential decay constant, but can have complicated decay dynamics including diffusion process. The dynamics then cannot be described by the rate equation, but by a diffusion equation considered to take place in the time range of 5–10 ps.

3.2. Electronic phase relaxation time between S_0 and S_1 states

To begin, a brief theoretical background is described so as to discuss the determination of the electronic phase relaxation time.

In the rotating reference frame, the time evolution of the elements of the density matrix ρ is described as two-electronic state system. The density matrix is corresponding two of the eigen states relevant to the optical transition resonant to the laser field. The electronic states in *trans*-polyacetylene is strongly coupled to the vibration. The eigen states between which transition is taking place are vibronic eigen states of the Hamiltonian considered to be solved without factorisation into vibrational and electronic eigen-state wave functions.

The two-electronic state system interacting with pump ($\boldsymbol{E}_{pu}(t)$)and probe ($\boldsymbol{E}_{pr}(t)$) fields is described by

$$\dot{\rho}_{ba}(\boldsymbol{r},t) = -\left(i\Omega + \frac{1}{T_2}\right)\rho_{ba}(\boldsymbol{r},t) + \frac{i}{\hbar}V_{ba}(\boldsymbol{r},t)N \tag{2}$$

$$\dot{\rho}_{bb}(\boldsymbol{r},t) - \dot{\rho}_{aa}(\boldsymbol{r},t) = -\frac{N-N_0}{T_1} + \frac{2i}{\hbar}[V^*_{ba}(\boldsymbol{r},t)\rho_{ba}(\boldsymbol{r},t) - V_{ba}(\boldsymbol{r},t)\rho^*_{ba}(\boldsymbol{r},t)] \tag{3}$$

The interaction potential $V_{ba}(\boldsymbol{r},t)$ is given by

$$V_{ba}(\boldsymbol{r},t) = -\mu[\boldsymbol{E}_{pu}(t)\exp(i\boldsymbol{k}_{pu}\boldsymbol{r}) + \boldsymbol{E}_{pr}(t)\exp(i\boldsymbol{k}_{pr}\boldsymbol{r})] \tag{4}$$

where μ is the transition dipole moment, T_1 and T_2 are the longitudinal and transverse electronic relaxation time, respectively, between states 1 and 2; $N = \rho_{bb}(\boldsymbol{r},t) - \rho_{aa}(\boldsymbol{r},t)$ is the population difference, and $N_0 = (\rho_{bb}(\boldsymbol{r},t) - \rho_{aa}(\boldsymbol{r},t))_0$ is the equilibrium population difference without the field; $\Omega = \omega_{ba} - \omega_1$ is the detuning between the pump field frequency ω_1 and the transition frequency ω_{ba}.

The time envelope function of the macroscopic polarization $\boldsymbol{P}^{(3)}_{pr}(t)$ in a molecular vibronic system propagating in the probe direction is given by the following [20]:

$$\begin{aligned}\boldsymbol{P}^{(3)}_{pr} = {} & [\rho_{bb}(\boldsymbol{r},t) - \rho_{aa}(\boldsymbol{r},t)]_0 \int_{-\infty}^{+\infty} dt_3 A_2(t_3)\left\{\boldsymbol{E}_{pr}(t-t_3)\int_{-\infty}^{+\infty} dt_2 A_1(t_2)\left[\boldsymbol{E}_{pu}(t-t_3-t_2)\int_{-\infty}^{+\infty} dt_1 A_2(t_1)\boldsymbol{E}^*_{pu}(t-t_3-t_2-t_1)\right.\right.\\ & \left. -\boldsymbol{E}^*_{pu}(t-t_3-t_2)\int_{-\infty}^{+\infty} dt_1 A_2(t_1)\boldsymbol{E}_{pu}(t-t_3-t_2-t_1)\right]\\ & +\boldsymbol{E}_{pu}(t-t_3)\int_{-\infty}^{+\infty} dt_2 A_1(t_2)\left[\boldsymbol{E}_{pr}(t-t_3-t_2)\int_{-\infty}^{+\infty} dt_1 A_2(t_1)\boldsymbol{E}^*_{pu}(t-t_3-t_2-t_1)\right]\\ & \left. -\boldsymbol{E}_{pu}(t-t_3)\int_{-\infty}^{+\infty} dt_2 A_1(t_2)\left[\boldsymbol{E}^*_{pu}(t-t_3-t_2)\int_{-\infty}^{+\infty} dt_1 A_2(t_1)\boldsymbol{E}_{pr}(t-t_3-t_2-t_1)\right] + \boldsymbol{E}_{pr}(t-t_3)\right\}\end{aligned} \tag{5}$$

Here, the initial condition is given by $A_1(t) = A_2(t) = 0$ $(t < 0)$

$$A_1(t) = \frac{2i\mu}{\hbar}\exp\left(\frac{-t}{T_1^{el}}\right) \times \exp(-i(\omega_v t + \tan^{-1}((\omega - \omega_e + \omega_v)T_{vib}))) \quad (t > 0) \tag{6}$$

$$A_2(t) = \frac{i\mu}{\hbar}\exp\left(\frac{-t}{T_2^{el}}\right)\exp(-i\Omega t)\exp\left(\frac{-t}{T_2^{vib}}\right) \times \exp(-i(\omega t + \tan^{-1}((\omega - \omega_e + \omega_v)T_{vib}))) \quad (t > 0) \tag{7}$$

Here T_{vib} is the vibrational period, T_2^{el} and T_2^{vib} are the electronic and vibrational dephasing times, respectively, and ω_e is the frequency corresponding to the 0–0 transition energy from the ground state to the electronic excited state.

Eq. (5) is the result of the perturbation of optical fields up to the third-order nonlinear susceptibility, and not the perturbation of vibration to the electronic transition due to the vibronic coupling. The vibronic coupling is fully taken into account in $\rho_{ab}(\boldsymbol{r},t)$ which is not the pure electronic polarization or electronic polarization with perturbative vibrational levels included in the direct product of the linear combination of the electronic wave functions coupled through the perturbative coupling up to some lower order vibronic coupling. Instead it is the vibronic polarization, where all orders of perturbation and fully taken into account.

The difference spectrum of the probe transmittance is found to have three distinct polarization components as described in Eq. (5). The difference spectrum corresponding to the first term is proportional to the level population changes induced by the pump pulse, which is detected when the probe pulse arrives. This level population term gives a signal due to incoherent process of population transfer from the ground state to the electronic excited state being coupled through dipole allowed electronic transition. In this incoherent term, coherent effects do not play an important role. This same term appears only after the onset of the pump pulse, as seen from Eqs. (6) and (7), which contribute only to the positive time region. The change in the transition probability due to the time-dependent Franck–Condon factor (Franck–Condon mechanism) or to the non-Condon effect (non-Condon mechanism) is associated with the motion of the wave packet [20–23]. Therefore, it is the only term which persists when the probe follows the pump and decays exponentially with time constant ${T_1}^{el}$.

The second term in Eq. (5) is proportional to the pump-induced polarization present when the probe pulse arrives at the same time as the pump pulse. The probe field interacts with this pump polarization to create a grating due to spatial modulation of the level populations. The pump field then interacts with the grating to create a polarization component spatially coherent with the probe field [20,24–26]. This term is called the "pump polarization coupling" term. It is effective only when the pump pulse overlaps the probe pulse in time, since it requires the presence of the pump field both before and after the arrival of the probe pulse.

The third term occurs because the presence of the pump field modifies the otherwise free decay of the probe-induced polarization. This term is called the "perturbed free induction decay" term. It persists when the probe precedes the pump, grows exponentially with time constant ${T_2}^{el}$ and becomes zero quickly at $t = 0$. Therefore this can be used in the determination of the electronic phase relax-

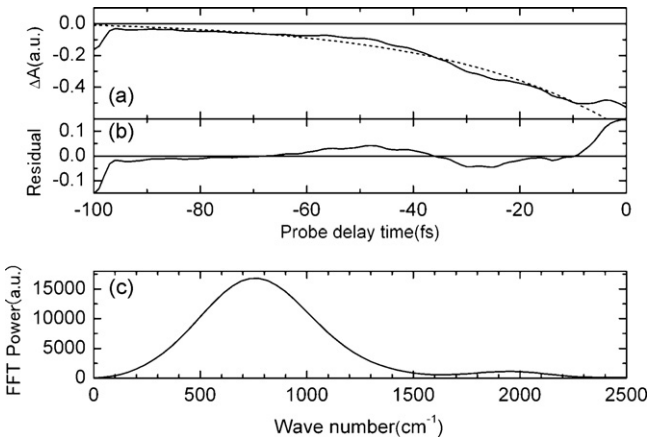

Fig. 3. $\Delta A(t)$ in negative-time region of t-PA at 1.88 eV: (a) the results are experiment (solid line) and fitted (dashed line) and (b) the difference between experimental and fitted data, associated with molecular vibrations. (c) FFT power spectrum of (b).

ation time. It can also be used to study vibrational phase relaxation in the electronic excited state(s) [27]. In the case t-PA studied in this paper, electron–hole pairs have very short lifetimes in forming excited states, and hence the vibrations in the excited state are difficult to detect.

As discussed above, in the time range when the probe pulse precedes the pump pulse, the probe delay time dependence of the signal provides information about the electronic polarization induced by the probe pulse. This time range is called the "negative-time" range in this paper. In this range, the pump pulse in the negative-time, by the electronic coherence grating and created by the probe light, induced coherent electronic polarization and pump field. Therefore, the signal lasts as long as the electronic coherence is maintained. The phase relaxation time of the relevant electronic states can be obtained from the delay time dependence in the negative time. From the spectral overlap relation between the absorption and laser in the present experiment, it is seen, as will be described below, that the relevant electronic states are the ground state and the excited state corresponding to the electron–hole pair.

The rate of dephasing $(1/T_2^{ele})$ obtained from the plot comprises three components given below,

$$\frac{1}{T_2^{ele}} = \frac{1}{2T_1^{ele}} + \frac{1}{T_2^{'ele}} + \frac{1}{T_2^{*ele}} \tag{8}$$

Here T_1^{ele} is the population decay time, and $T_2^{'ele}$ and T_2^{*ele} are respectively the pure electronic dephasing time and the electronic phase relaxation time due to inhomogeneous broadening. In order to discuss the pure phase relaxation time constant $T_2^{'ele}$, we must know more about T_2^{*ele}. Here, for simplicity, we assume $T_2^{'ele} = \infty$. Since the value of T_2^{*ele} is very short, it can safely be considered that $T_2^{*ele} \gg T_2^{ele}$, and the assumption is considered to be well-satisfied. From the analysis of the plot shown in Fig. 3(a), the electronic dephasing time was found to be $T_2^{ele} = 32 \pm 2$ fs. Then, from the shortest population decay time $T_1^{ele} = \tau_1 = 66 \pm 20$ fs determined in the previous section, the *pure* electronic dephasing time is determined to be $T_2^{'ele} = 62 \pm 19$ fs. Therefore, it can be concluded that 51% of the phase decay is due to a pure dephasing process and 49% is due to population decay resulting from electronic relaxation associated with extremely fast dissociation of bound solitons to form pairs of spatially separated solitons.

Fig. 3(a) shows plots of the decay in the negative time, from which a 32 fs decay time constant was determined, and the fitted curve of the decay function. It also depicts the oscillating component and its Fourier power spectrum, which has peak frequency of 773 cm^{-1} corresponding to the breather mode frequency. From the

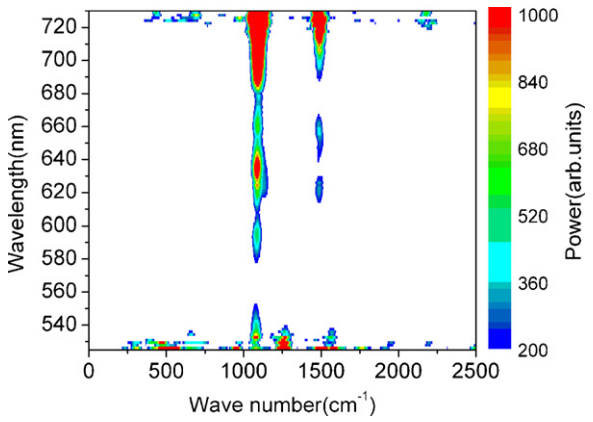

Fig. 4. Two-dimensional display of FFT power spectra of t-PA.

width of the power spectrum of the mode, the dephasing time of the vibrational mode was estimated to be $T_2^{ex.vib} = 37 \pm 5$ fs.

3.3. Molecular vibration spectra

Probe delay time (t) dependent change, $\delta\Delta A(\omega, t)$ in $\Delta A(\omega, t)$, is due to molecular vibration. Fig. 4 shows the two-dimensional (ω, t) display of the fast Fourier transform (FFT) power spectra of real-time traces of $\Delta A(\omega, t)$ probed at the 128 photon energies used to obtain Fig. 2. The peak positions of the FFT amplitude due to C—C and C=C stretching modes were 1089 ± 6 cm^{-1} and 1487 ± 10 cm^{-1}, respectively. The FFT cosine phases of C—C and C=C stretching modes are $(0.9 \pm 0.3)\,\pi$ and $(0.7 \pm 0.4)\,\pi$ radian, respectively, in a photon energy range indicating that these modes are created initially in the excited state. The FWHM of the peaks of each mode were 59 ± 2 cm^{-1} and 70 ± 3 cm^{-1}, respectively, corresponding to the vibrational dephasing times of 570 ± 24 fs and 480 ± 14 fs, respectively. The dephasing times of both modes are close to the above mentioned recombination time (565 ± 50 fs) of a charged soliton pair. This indicates that the dephasing of vibrational modes is determined partly by the recombination of the soliton pair and partly by the pure dephasing with nearly equal contribution.

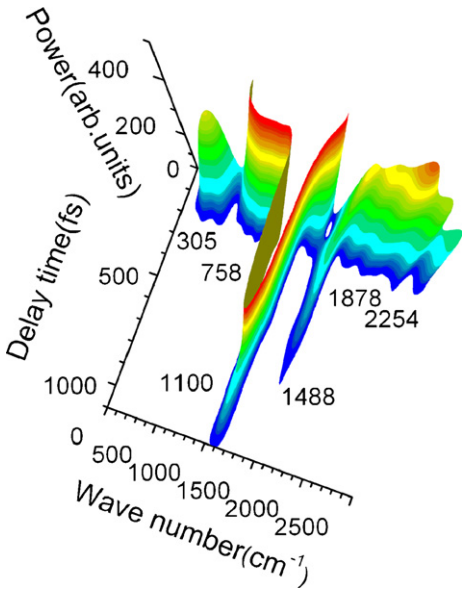

Fig. 5. Three-dimensional display of spectrogram spectra of t-PA at 1.71 eV.

3.4. Modulated phonon dynamics induced by the breather soliton

The results of the spectrogram analysis [28–30] of the real-time trace at 1.71 eV are shown in Fig. 5. The probe delay time dependent Fourier amplitude reveals the time evolution of C—C and C=C stretching modes with $1100 \pm 8\,cm^{-1}$ and $1488 \pm 8\,cm^{-1}$, respectively. In addition to the main skeleton oscillation, there exist four peaks at 305 cm^{-1}, 757 cm^{-1}, 1877 cm^{-1}, and 2254 cm^{-1} with an uncertainty of $\pm 8\,cm^{-1}$. The separation between the main bands and corresponding sidebands is $770 \pm 40\,cm^{-1}$ in all four cases. This frequency separation corresponds to a modulation period of 43 ± 3 fs, which is consistent with the theoretically predicted (33–50 fs) for the breather period [9–11] and the previously observed (44 ± 3 fs) [2]. In the present work, these sidebands were observed over the whole photon energy range from 1.70 eV to 2.35 eV, which is considered to be the tail of the breather absorption with a peak located around 1.03 eV. In all cases, the lifetime of the sideband amplitude is about 60 fs, which is within experimental errors in agreement with the electronic dephasing time of 61 ± 14 fs. The coincidence is explained in the following discussion.

The profile of the spectrogram from 10 fs to 90 fs in increments of 20 fs is plotted in Fig. 6(a). The peak FFT amplitude of the C—C stretching mode shifts from 1155 cm^{-1} to 1095 cm^{-1} with time evolution, while that of the C=C stretching mode shifts from 1488.5 cm^{-1} to 1503 cm^{-1}. Our scenario of the primary processes of photoexcitation follows the steps proposed in earlier theoretical work [31,32]. The electron–hole pair formed by the photoexcitation associated with a localized breather mode relaxes to a spatially separated pair of charged solitons with a localized breather mode. The observed frequency shifts are interpreted as a consequence of the coupling of the breather with the charged solitons. In the following, the SSH Hamiltonian model [3,4] is used to describe above scenario. The model Hamiltonian is given as follows:

$$H = -\sum_{n,s}[t_0 + \alpha(u_n - u_{n+1})][c^{\dagger}_{n+1,s}c_{n,s} + c^{\dagger}_{n,s}c_{n+1,s}] + \frac{K}{2}\sum\nolimits_n (u_n - u_{n+1})^2 + \frac{M}{2}\sum_n \dot{u}_n^2 \quad (9)$$

where u_n is the displacement of nth CH group in the polymer chain, t_0 is the π band width, α is the electron–phonon coupling, K is the spring constant, and M is the mass of each CH group. $c^{\dagger}_{n,s}$ and $c_{n,s}$ are, respectively, the creation and annihilation operators of a π electron in the nth site with spin s. Based on this Hamiltonian, the classical equations of motion for order parameters $\bar{\psi}_n(t) \equiv (-1)^n u_n/u_0$, and velocities, $\dot{\bar{\psi}}_n$ can be derived [10]. Here $u_0 = 0.04$ Å, assuming that the change in bond length due to dimerization from the non-dimerized structure (that is, all bond orders are 1.5) is 0.08 Å [9]. Frequencies of the single and double bonds are determined exper-

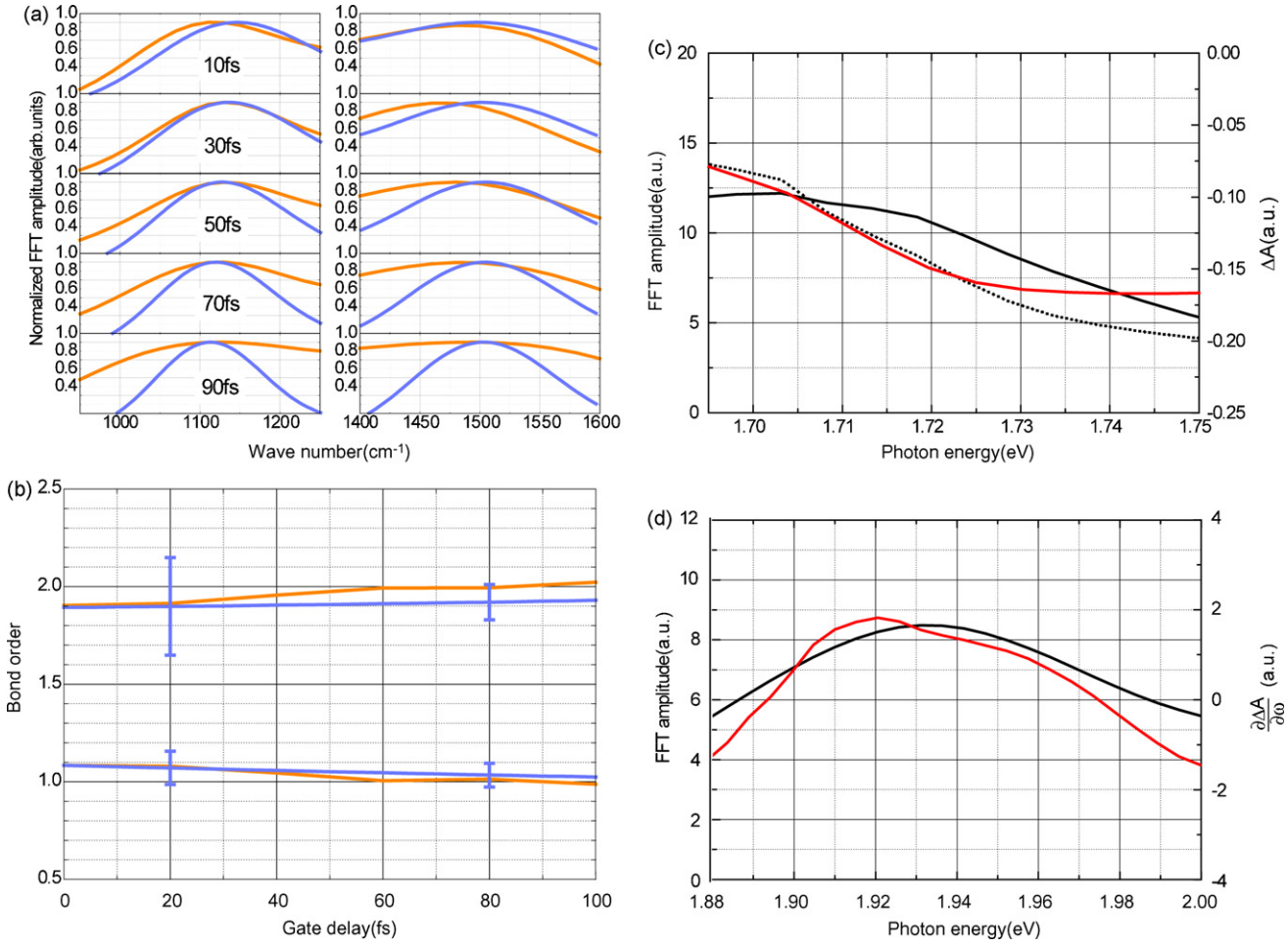

Fig. 6. Time traces and photon energy dependence of FFT amplitudes of C—C, C=C stretching and breather modes: (a) the results of experiment (blue line) and calculated (yellow line) time traces of FFT amplitude of C—C and C=C stretching modes, (b) the time trace of bond order, (c) the probe photon energy dependence of FFT amplitude of sidebands of the C=C stretching mode (solid and dashed black lines correspond to the lower and higher sidebands, respectively) and 0th derivative of $\Delta A(\omega, t)$ with respect to photon energy (red line) at 50 fs, and (d) the probe photon energy dependence of C=C stretching mode (black line) and the 1st derivative of $\Delta A(\omega, t)$ with respect to photon energy (red line) at 100 fs. (For interpretation of the references to color in this figure legend, the reader is referred to the web version of the article.)

imentally to be 1095 cm^{-1} and 1503 cm^{-1}, respectively. Calculated results and the observed data are shown in Fig. 6(a), revealing that the peak of the single bond red-shifts, while the peak of the double bond blue-shifts. It is also shown that the initially localized excitation, with a peak having an order parameter of −2, results in the two peaks being closer to each other. The time trace of the bond order is estimated from both experimental and calculated data [33] (Fig. 6(b)). The figure shows that the bond order of each bond exceeds 1 on the lower order side and is less than 2 on the higher side at the moment of electron–hole pair generation.

Recently, Tretiak et al. found that the breather and the C=C stretching modes mainly modulate the intensities (transition dipoles and oscillator strength) and transition energies, respectively [13,14]. To verify these calculations, the 0th and 1st derivative of ΔA with respect to photon energy were compared with the probe photon energy dependence of FFT amplitude of spectrogram analysis (Fig. 6(c) and (d)). The 0th and 1st derivative of ΔA correspond to the modulation of the transition intensity and that of the electronic transition energy, respectively. These results are consistent with the prediction made by Tretiak and others [13,14].

4. Conclusions

In conclusion, the prediction of [9–11] that after photoexcitation, the electron–hole pair relaxes via a breather mode with an electron–hole pair lifetime of 33–50 fs, have been directly verified. The electronic dephasing time which was determined by the ΔA in the negative-time range revealed that 51% is due to a pure electronic dephasing process and 49% is due to population decay resulting from electronic relaxation associated with extremely fast dissociation of a bound soliton to a pair of spatially separated charged solitons. We could also determine the ultrafast phonon dynamics induced by the breather in *t*-PA, including amplitude modulation, frequency modulation and frequency shifts of C—C and C=C stretching modes. Calculations with the SSH Hamiltonian reproduced the time trace of the bond order of the C—C bonds in the polyacetylene. As also theoretically predicted, the breather and the C=C stretching modes were found mainly to modulate the transition intensity and transition energy, respectively.

Acknowledgements

The authors wish to thank Dr. A.R. Bishop, Dr. S. Tretiak, and their group members for their fruitful comments. This work was partly supported by a grant from the Ministry of Education (MOE) in Taiwan under the ATU Program at National Chiao Tung University. A part of this work was performed under the joint research project of the Institute of Laser Engineering, Osaka University under Contract No. B1-27.

References

[1] G.S. Kanner, et al., Synth. Met. 16 (2001) 71.
[2] S. Adachi, V.M. Kobryanskii, T. Kobayashi, Phys. Rev. Lett. 89 (2002) 027401–27411.
[3] W.P. Su, J.R. Schrieffer, A.J. Heeger, Phys. Rev. Lett. 42 (1979) 1698.
[4] W.P. Su, J.R. Schrieffer, A.J. Heeger, Phys. Rev. B 42 (1980) 2099.
[5] A.J. Heeger, et al., Rev. Mod. Phys. 60 (1988) 781.
[6] M. Yoshizawa, et al., J. Phys. Soc. Jpn. 56 (1987) 768.
[7] S. Takeuchi, T. Masuda, T. Kobayashi, J. Chem. Phys. 105 (1996) 2859.
[8] C.V. Shank, et al., Phys. Rev. Lett. 49 (1982) 1660.
[9] W.P. Su, J.R. Schrieffer, Proc. Natl. Acad. Sci. U.S.A. 77 (1980) 5626.
[10] A.R. Bishop, et al., Synth. Met. 9 (1984) 223.
[11] M. Sasai, H. Fukutome, Prog. Theor. Phys. 79 (1987) 61.
[12] S.R. Phillpot, A.R. Bishop, B. Horovitz, Phys. Rev. B 40 (1989) 1839.
[13] S. Tretiak, et al., Phys. Rev. B 70 (2004) 233203–233211.
[14] S. Tretiak, et al., Proc. Natl. Acad. Sci. U.S.A. 100 (2003) 2185.
[15] V.M. Kobryanskii, Rapra Rev. Rep. 10, No. 6, Rep. 114, 2000.
[16] C. Chudoba, E.T.J. Nibbering, T. Elsaesser, J. Phys. Chem. A 103 (1999) 5625.
[17] A. Shirakawa, I. Sakane, T. Kobayashi, Opt. Lett. 23 (1998) 1292.
[18] A. Baltuska, A.T. Fuji, T. Kobayashi, Opt. Lett. 27 (2002) 306.
[19] L. Luer, et al., Chem. Phys. Lett. 444 (2007) 61.
[20] C.H. Cruz, et al., IEEE J. Quantum Electron. 24 (1988) 261.
[21] T. Kobayashi, Z. Wang, T. Otsubo, J Phys. Chem. A 111 (2007) 12985.
[22] T. Kobayashi, Z. Wang, I. Iwakura, New J. Phys. 10 (2008) 065009.
[23] T. Kobayashi, Z. Wang, New J. Phys. 10 (2008) 065013.
[24] C.H. Brito Cruz, et al., Chem. Phys. Lett. 132 (1986) 341.
[25] C.V. Shank, et al., in: G.R. Fleming, A.E. Siegman (Eds.), Ultrafast Phenomena V, Springer-Verlag, Berlin, 1986, p. 179.
[26] J.J. Baumberg, B. Huttner, R.A. Taylor, J.F. Ryan, Phys. Rev. B 48 (1993) 4695.
[27] T. Kobayashi, et al., Phys. Rev. Lett. 101 (2008) 037402–37411.
[28] T. Kobayashi, T. Saito, H. Ohtani, Nature 414 (2001) 531.
[29] T. Kobayashi, et al., Chem. Phys. Lett. 321 (2000) 385.
[30] M.J.J. Vrakking, D.M. Villeneuve, A. Stolow, Phys. Rev. A 54 (1996) R37.
[31] A.R. Bishop, et al., Phys. Rev. Lett. 52 (1984) 671.
[32] S. Mukamel, S. Tretiak, T. Wagersreiter, V. Chernyak, Science 277 (1997) 781.
[33] R.H. Baughman, J.D. Witt, K.C. Yee, J. Chem. Phys. 60 (12) (1974) 4755.